Supplementary materials for

# Climate-mediated spatiotemporal variability in the terrestrial productivity across Europe

Xiuchen Wu[§*], Miguel D. Mahecha[§*], Markus Reichstein[§], Philippe Ciais[¶], Martin Wattenbach[†], Flurin Babst[‡ǂ], David Frank[ǂǁ], Christian Zang[‼]

[§]Max Planck Institute for Biogeochemistry, Hans-Knoll-Str. 10, D-07745 Jena, Germany

[¶]CEA-CNRS-UVSQ, UMR8212-Laboratoire des Sciences du Climat et de l'Environnement (LSCE), Orme des Merisiers, 91191, Gif-Sur-Yvette, France

[†]Helmholtz Centre Potsdam GFZ German Research Centre For Geosciences, Deutsches GeoForschungsZentrum GFZ, Telegrafenberg, 14473, Potsdam, Germany

[‡]Swiss Federal Research Institute WSL, Dendroclimatology, Zürcherstrasse 111, Birmensdorf 8903, Switzerland

[ǂ]Laboratory of Tree-Ring Research, University of Arizona, 1215 E Lowell St, Tucson AZ 85721, USA

[ǁ]Oeschger Centre for Climate Change Research, University of Bern, Bern, Switzerland

[‼]Technische Universität Munchen, Hans-Carl-von-Carlowitz-Platz 2, 85354, Freising, Germany

[*]Correspondence:

Xiuchen Wu

Tel: +33 (0) 1 69 08 77 24; Fax: +33 (0) 1 69 08 77 16; E-mail: wuxiuchen2000@163.com

Miguel D. Mahecha

Tel: +49 3641 576265; Fax: +49 3641 577200; E-mail: mmahecha@bgc-jena.mpg.de

This file contains figure S1-S21 and references.

# Figure S1

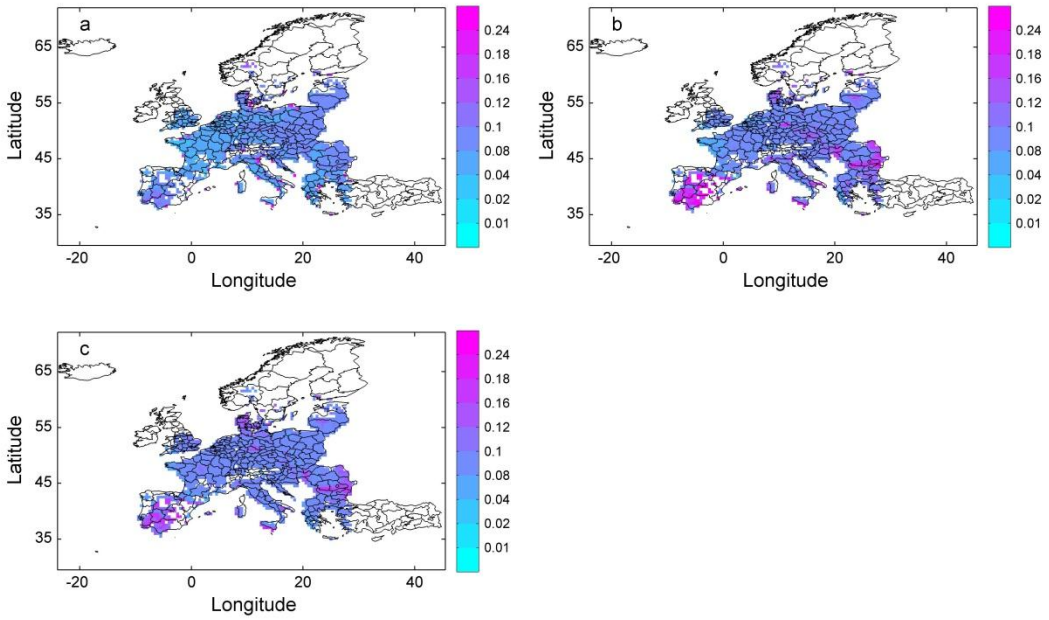


Figure S1. Spatial patterns of the coefficients of variation (CV) of the detrended March-June summed NDVI (a), GPP (b), and FAPAR (c) during 1982-2008. Blank region indicates that there is no crop yield records or with very low (< 5%) fraction of croplands in those pixels.

## Figure S2

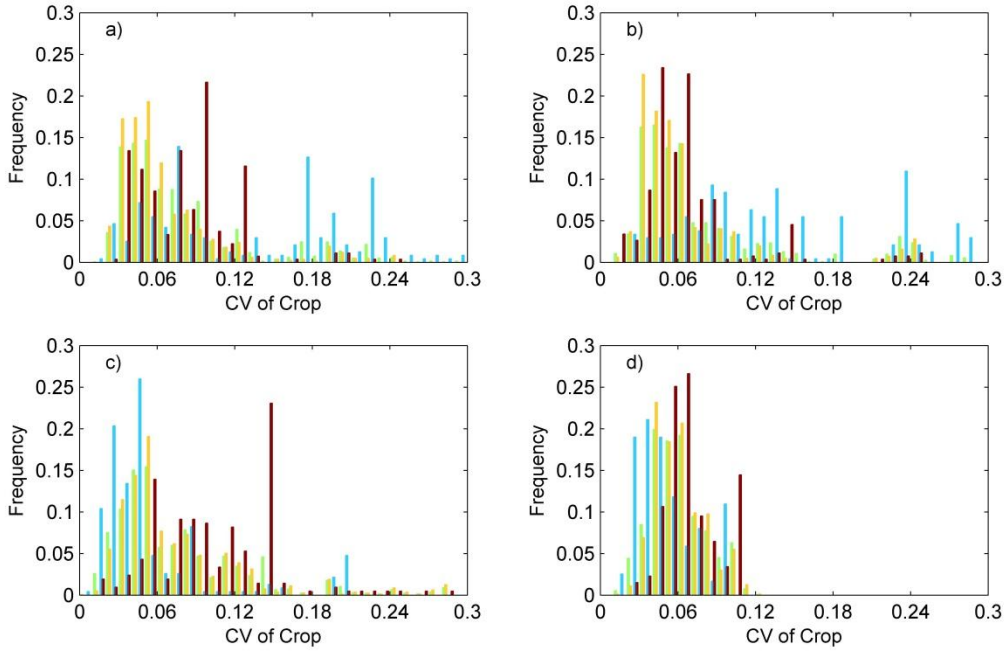


Figure S2. Frequency distribution of coefficients of variation (CV) of the detrended crop yield data in Europe (green bars), and climate zones of Cf (orange bars), Cs (blue bars) and Df (brown bars), which are derived from Köppen-Geiger climate classification, for barley (a), wheat (b), grain maize (c) and potatoes (d) during 1975-2009.

**Figure S3.**

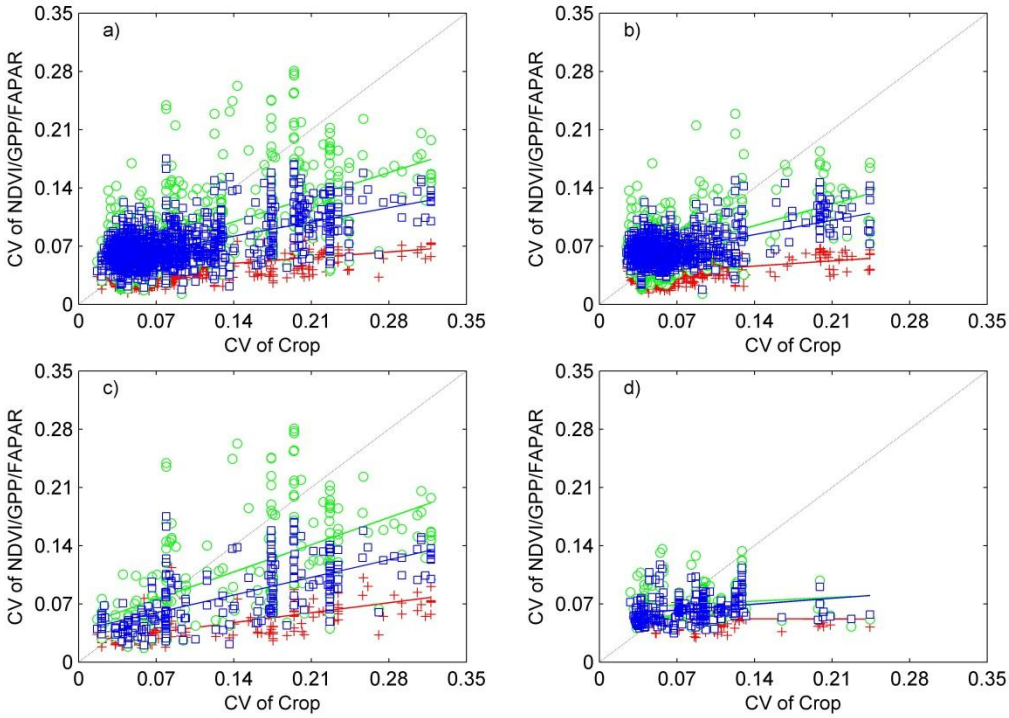


Figure S3. Comparisons of coefficients of variation of barley yield with coefficients of variation of March-June summed NDVI (red crosses), GPP (green circles), and FAPAR (blue squares) in Europe (a) and climate zones of Cf (b), Cs (c) and Df (d), respectively.

**Figure S4.**

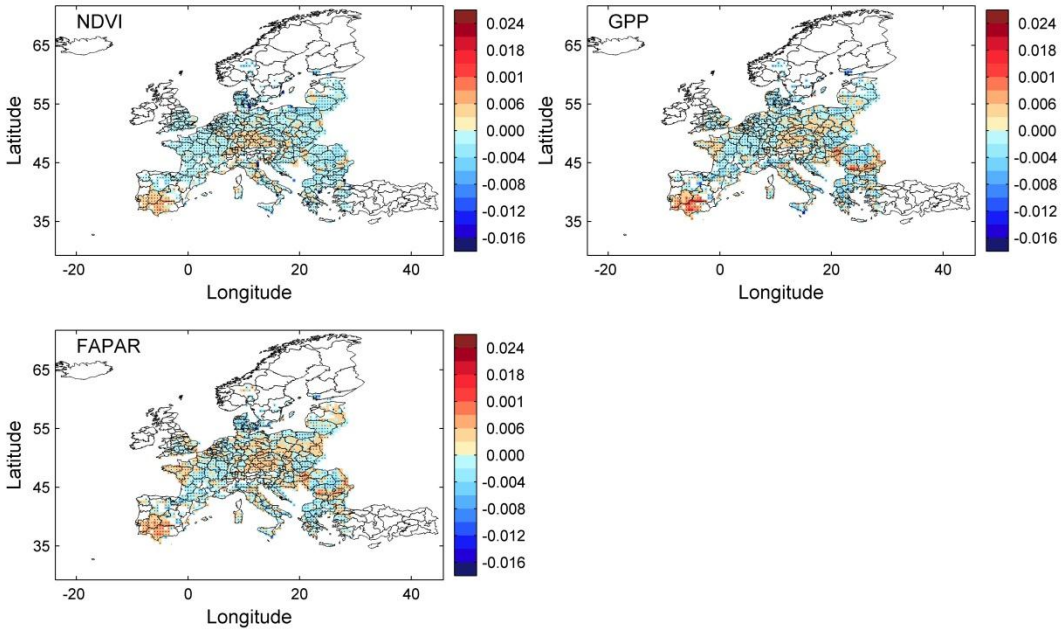


Figure S4. Spatial patterns of the estimated trends in the moving coefficients of variation (CV) of the detrended March-June summed NDVI, GPP and FAPAR calculated using a 10-yr sliding window with 1-yr lag during 1982-2008. The trends in the moving CV are estimated by the Theil-Sen slope method (Yue *et al.*, 2002). Significant trends were marked by black points. Blank region indicates that there is no crop yield records or with very low (< 5%) fraction of croplands in those pixels.

## Figure S5

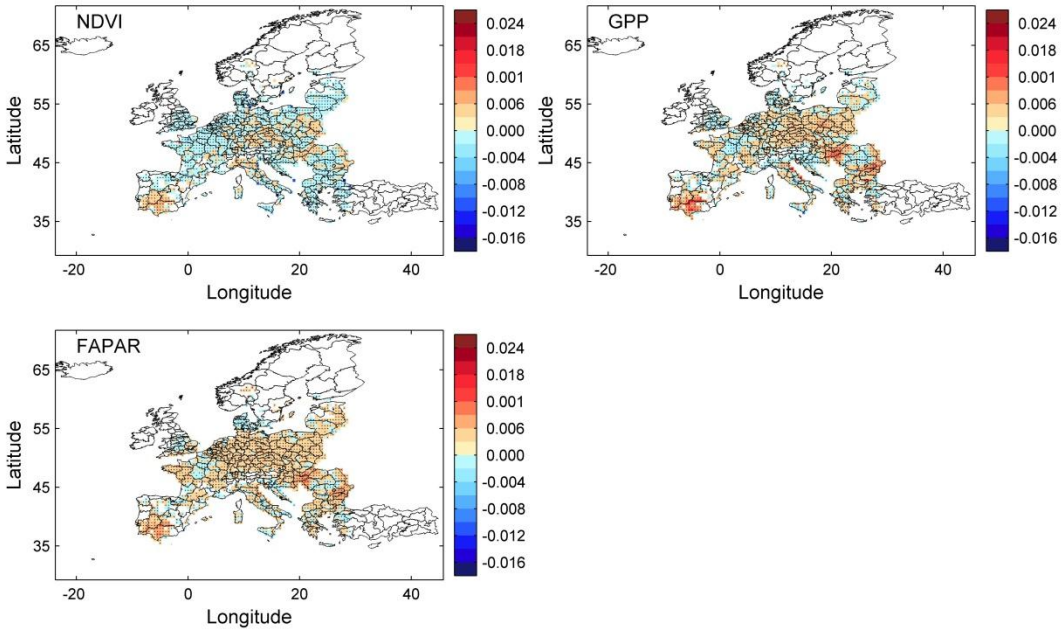


Figure S5. Spatial patterns of the estimated trends in the moving coefficients of variation (CV) of the detrended March-September summed NDVI, GPP and FAPAR calculated using a 10-yr sliding window with 1-yr lag during 1982-2008. The trends in the moving CV are estimated by the Theil-Sen slope method (Yue *et al.*, 2002). Significant trends were marked by black points. Blank region indicates that there is no crop yield records or with very low (< 5%) fraction of croplands in those pixels.

## Figure S6

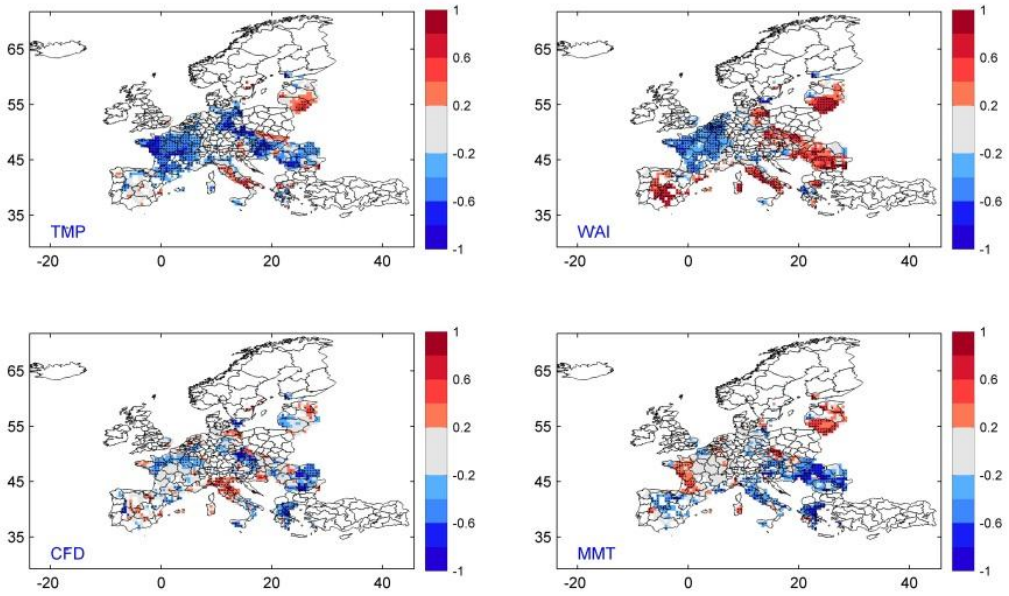


Figure S6. Response function coefficients between wheat yield and mean growing season temperature (TMP), total growing season water availability index (WAI) and consecutive frost days (CFD) and mean growing season maximum of daily maximum mean temperature (MMT). Significant response function coefficients between wheat yield and climate are marked by black points. Blank regions indicate that there is no crop yield records or with very low (< 5%) fraction of croplands in those pixels.

## Figure S7

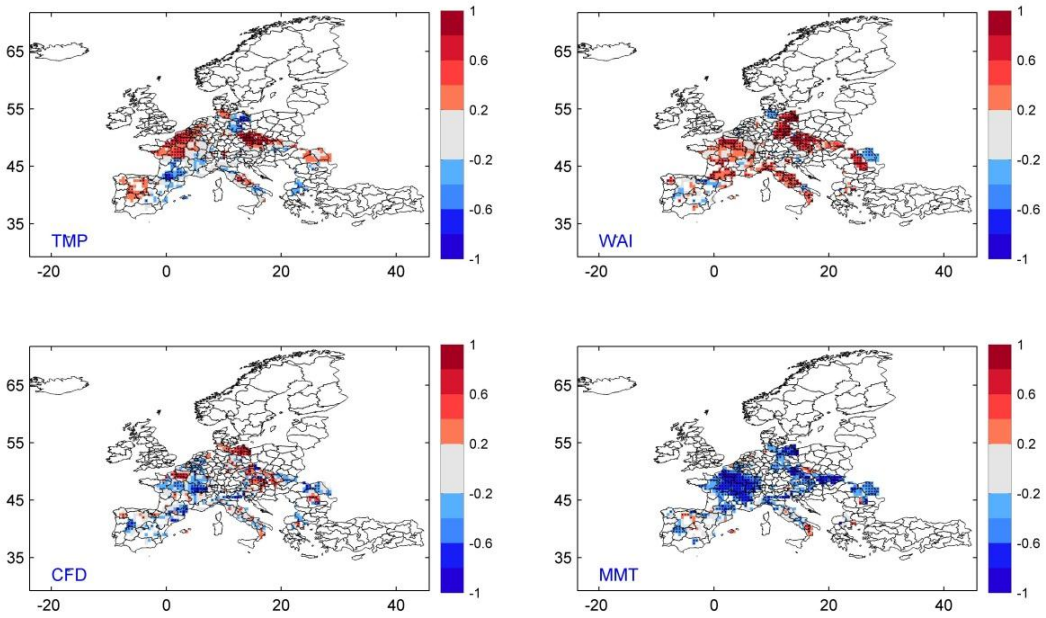


Figure S7. Response function coefficients between grain maize yield and mean growing season temperature (TMP), total growing season water availability index (WAI) and consecutive frost days (CFD) and mean growing season maximum of daily maximum mean temperature (MMT). Significant response function coefficients between grain maize yield and climate are marked by black points. Blank regions indicate that there is no crop yield records or with very low (< 5%) fraction of croplands in those pixels.

## Figure S8

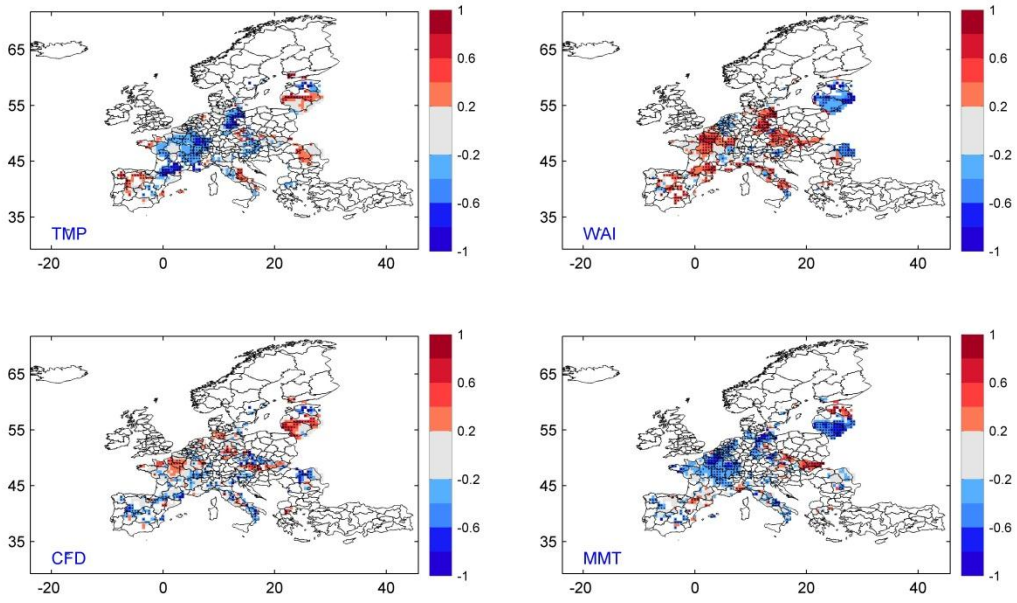


Figure S8. Response function coefficients between potato yield and mean growing season temperature (TMP), total growing season water availability index (WAI) and consecutive frost days (CFD) and mean growing season maximum of daily maximum mean temperature (MMT). Significant response function coefficients between potato yield and climate are marked by black points. Blank regions indicate that there is no crop yield records or with very low (< 5%) fraction of croplands in those pixels.

## Figure S9

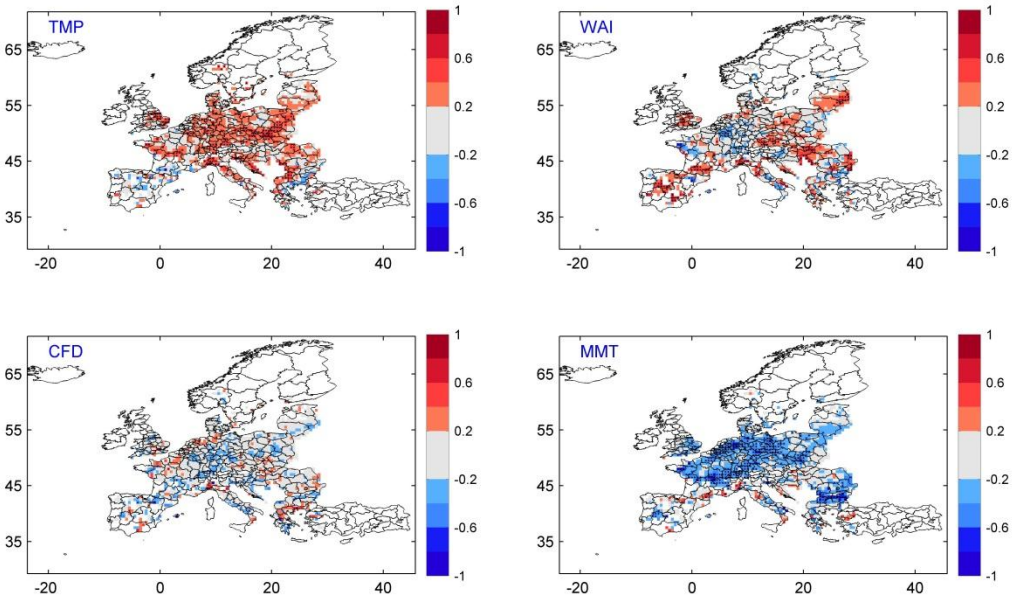


Figure S9. Response function coefficients between March-September summed NDVI and mean March-September temperature (TMP), total March-September water availability index (WAI) and consecutive frost days (CFD) and mean March-September maximum of daily maximum mean temperature (MMT). Significant response function coefficients between NDVI and climate are marked by black points. Blank regions indicate that there is no crop yield records or with very low (< 5%) fraction of croplands in those pixels.

## Figure S10

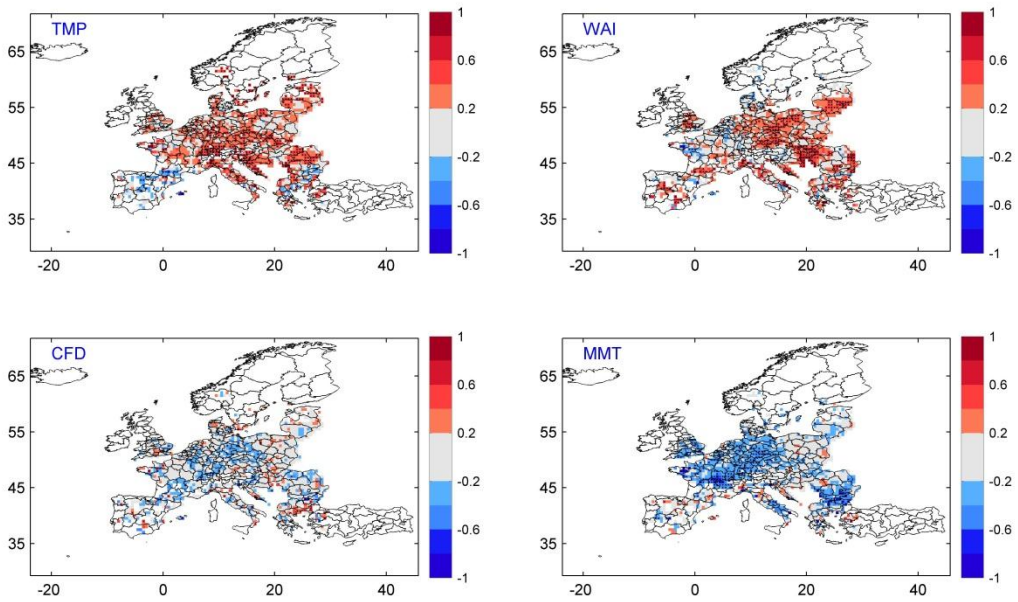


Figure S10. Response function coefficients between March-September summed GPP and mean March-September temperature (TMP), total March-September water availability index (WAI) and consecutive frost days (CFD) and mean March-September maximum of daily maximum mean temperature (MMT). Significant response function coefficients between GPP and climate are marked by black points. Blank regions indicate that there is no crop yield records or with very low (< 5%) fraction of croplands in those pixels.

## Figure S11

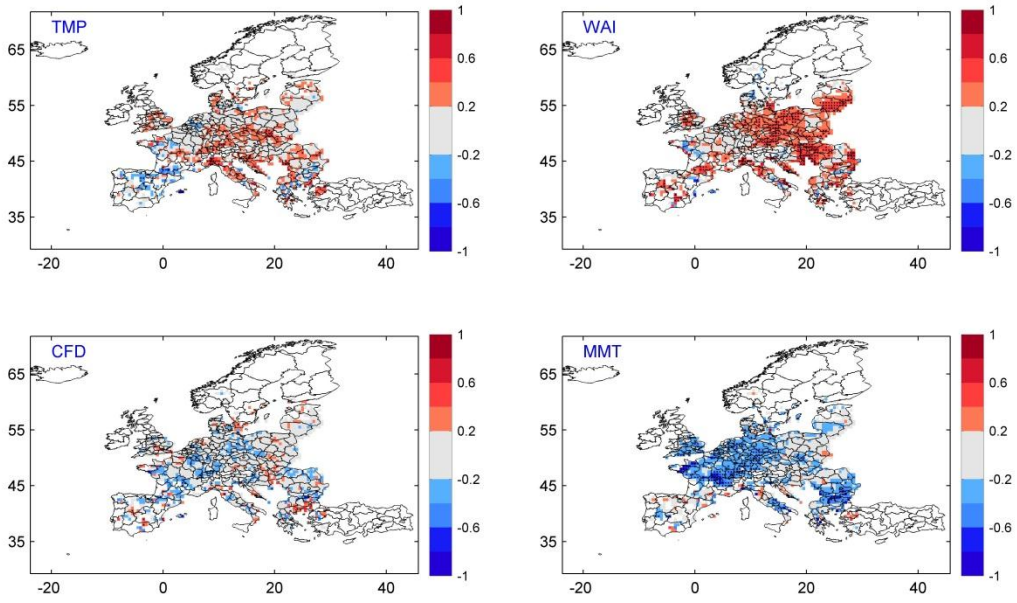


Figure S11. Response function coefficients between March-September summed FAPAR and mean March-September temperature (TMP), total March-September water availability index (WAI) and consecutive frost days (CFD) and mean March-September maximum of daily maximum mean temperature (MMT). Significant response function coefficients between FAPAR and climate are marked by black points. Blank regions indicate that there is no crop yield records or with very low (< 5%) fraction of croplands in those pixels.

## Figure S12

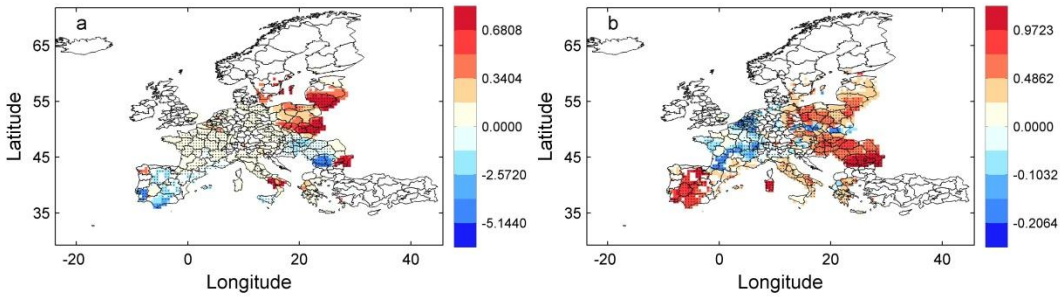


Figure S12. Spatial patterns of the climate sensitivity of wheat yield to the mean growing-season temperature (a) and total growing season water availability index (b) estimated by the slope of linear regression during 1975-2009. Significant slopes were marked by black points. Blank regions indicate that there is no crop yield records or with very low (< 5%) fraction of croplands in those pixels.

## Figure S13

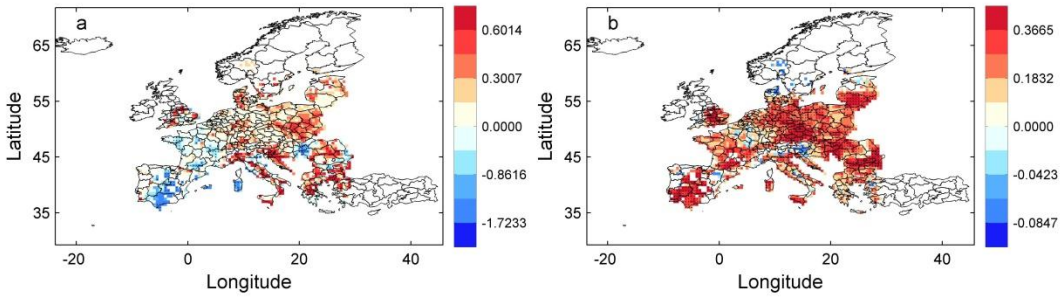


Figure S13. Spatial patterns of the climate sensitivity of March-September summed FAPAR to the mean March-September temperature (a) and total March-September water availability index (b) estimated by the slope of linear regression during 1982-2008. Significant slopes were marked by black points. Blank regions indicate that there is no crop yield records or with very low (< 5%) fraction of croplands in those pixels. Consistent patterns are also observed for March-September summed NDVI and GPP (data are not shown here).

## Figure S14

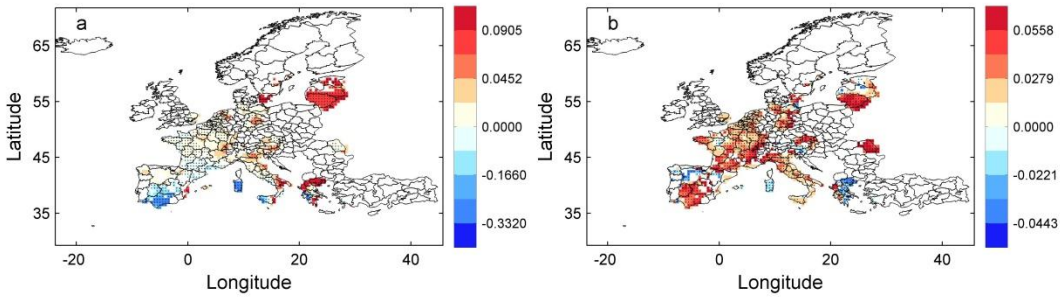


Figure S14. Spatial patterns of the linear trends in moving climate sensitivities of wheat yield to the mean growing-season temperature (a) and total growing season water availability index (b) estimated by the Theil-Sen slope method using a 10-yr sliding window with 1-yr lag during 1975-2009. Significant trends were marked by black points. Blank regions indicate that there is no crop yield records or with very low (< 5%) fraction of croplands in those pixels.

## Figure S15

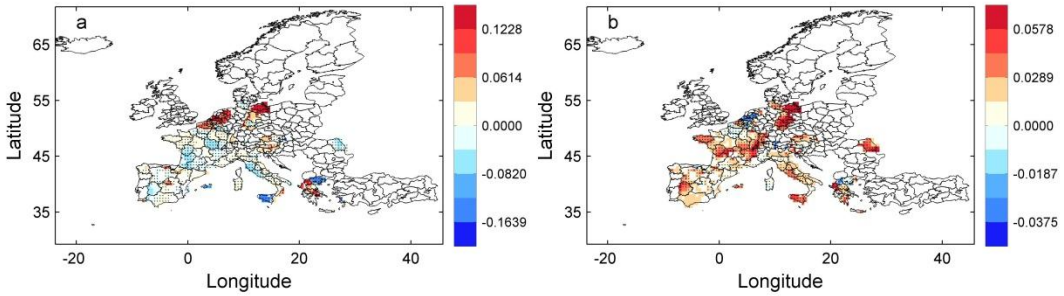


Figure S15. Spatial patterns of the linear trends in moving climate sensitivities of grain maize yield to the mean growing-season temperature (a) and total growing season water availability index (b) estimated by the Theil-Sen slope method using a 10-yr sliding window with 1-yr lag during 1975-2009. Significant trends were marked by black points. Blank regions indicate that there is no crop yield records or with very low (< 5%) fraction of croplands in those pixels.

## Figure S16

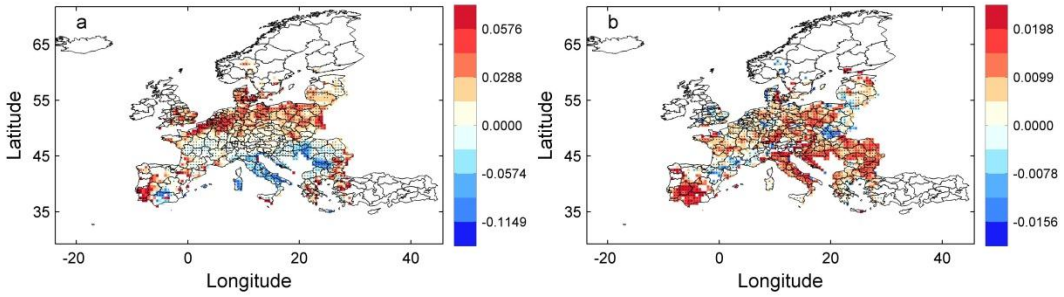


Figure S16. Spatial patterns of the linear trends in moving climate sensitivities of March-September summed NDVI to mean March-September temperature (a) and total March-September water availability index (b) estimated by the Theil-Sen slope method using a 10-yr sliding window with 1-yr lag during 1982-2008. Significant trends were marked by black points. Blank regions indicate that there is no crop yield records or with very low (< 5%) fraction of croplands in those pixels.

## Figure S17

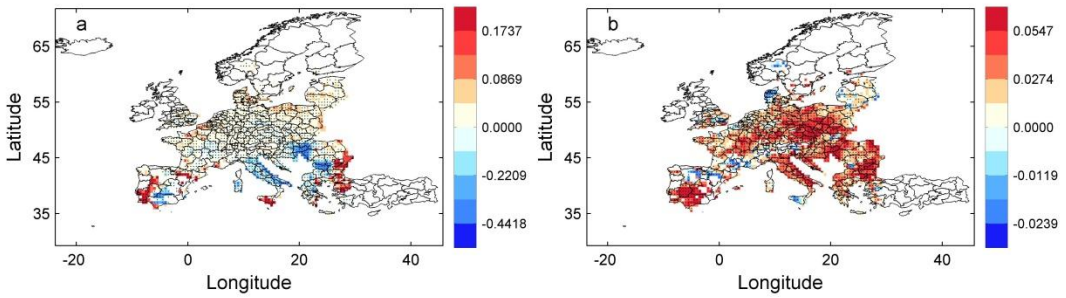


Figure S17. Spatial patterns of the linear trends in moving climate sensitivities of March-September summed GPP to mean March-September temperature (a) and total March-September water availability index (b) estimated by the Theil-Sen slope method using a 10-yr sliding window with 1-yr lag during 1982-2008. Significant trends were marked by black points. Blank regions indicate that there is no crop yield records or with very low (< 5%) fraction of croplands in those pixels.

## Figure S18

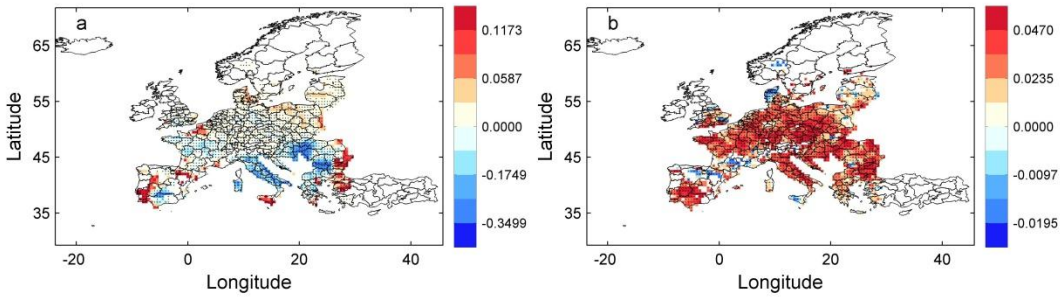


Figure S18. Spatial patterns of the linear trends in moving climate sensitivities of March-September summed FAPAR to mean March-September temperature (a) and total March-September water availability index (b) estimated by the Theil-Sen slope method using a 10-yr sliding window with 1-yr lag during 1982-2008. Significant trends were marked by black points. Blank regions indicate that there is no crop yield records or with very low (< 5%) fraction of croplands in those pixels.

## Figure S19

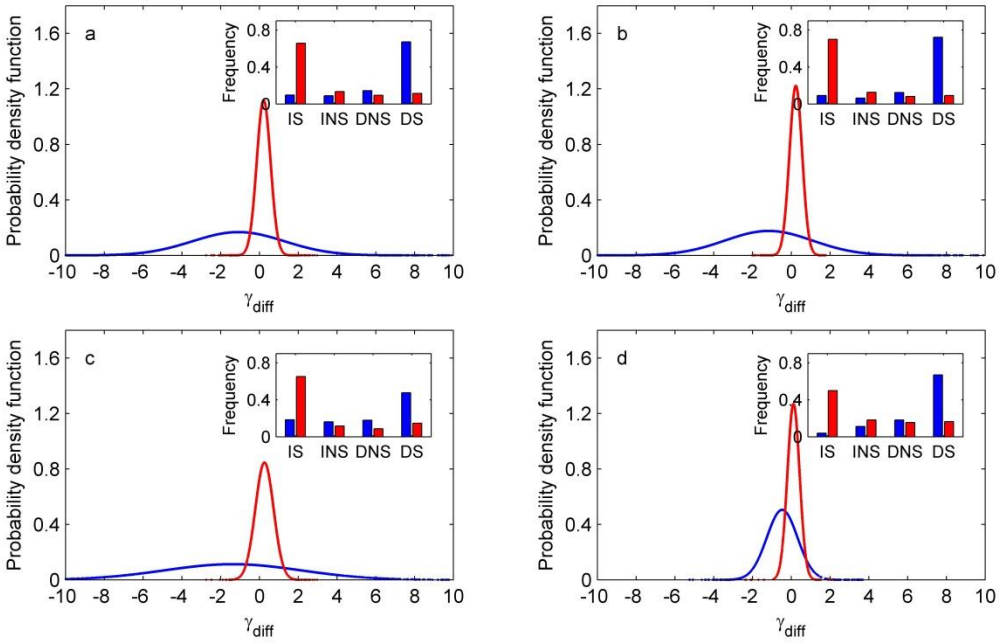


Figure S19. Probability density function for the differences of moving climate sensitivities of March-September summed GPP to mean March-September temperature (blue line) and total March-September water availability index (red line) between 1995-2008 and 1982-1995 for Europe (a), and climate zones Cf (b), Cs (c), and Df (d). The inlet shows the percentages of pixels suffering the four different trend types (significantly increasing, IS; increasing but not significant, INS; decreasing but not significant, DNS; significantly decreasing, DS) for climate sensitivities of GPP to mean March-September temperature (blue bars) and total March-September water availability index (red bars). Consistent patterns are also observed from the perspectives of NDVI and FAPAR (data are not shown).

## Figure S20.

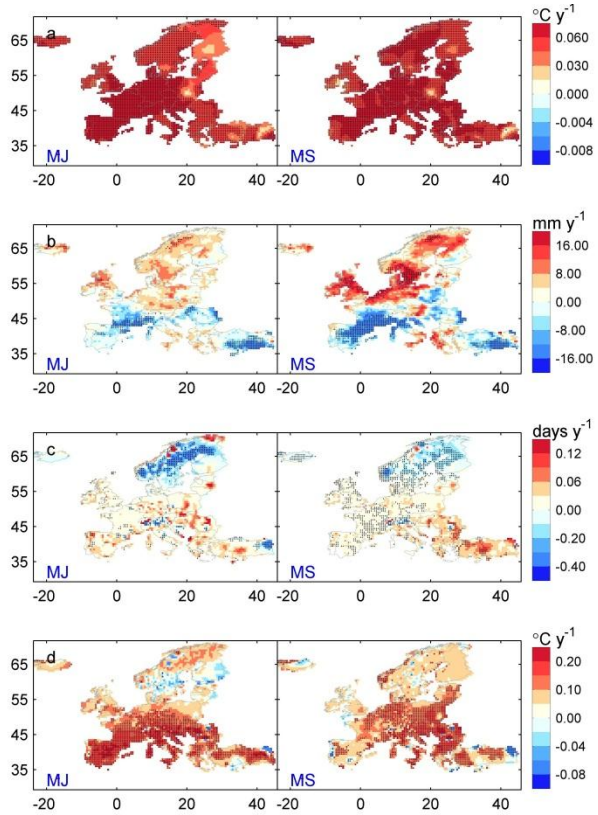


Figure S20. Linear trends in seasonal (MJ: March-June and MS: March-September) temperature (a), water availability index (b), consecutive frost days (c) and maximum of daily maximum mean temperature (d) during 1975-2009, as estimated by the linear regression. Significant ($p < 0.05$) trends were marked by black points.

**Figure S21.**

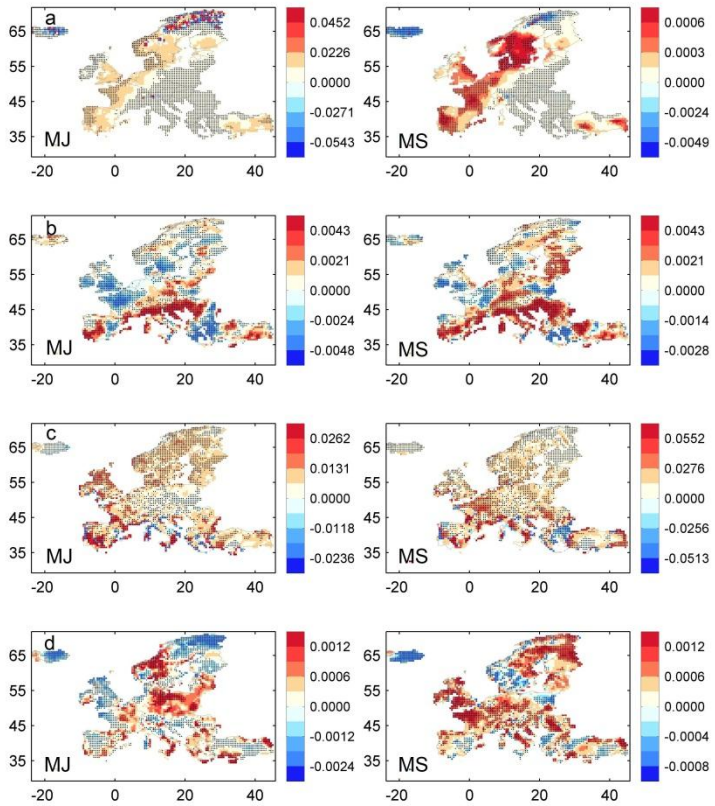


Figure S21. Linear trends in the moving coefficients of variation (CV) of the seasonal (MJ: March-June and MS: March-September) temperature (a), water availability index (b), consecutive frost days (c) and maximum of daily maximum mean temperature (d), as estimated by the Theil-Sen slope method using a 10-yr sliding window with 1-yr lag during 1975-2009. Significant ($p < 0.05$) trends were marked by black points.

## References

Yue S, Pilon P, Phinney B, Cavadias G (2002) The influence of autocorrelation on the ability to detect trend in hydrological series. *Hydrological Processes,* 16, 1807-1829.